

Article

Modeling and Optimization of a Green Process for Olive Mill Wastewater Treatment

Fatma Fakhfakh ¹, Sahar Raissi ¹, Karim Kriaa ², Chemseddine Maatki ³ , Lioua Kolsi ^{4,*}  and Bilel Hadrich ² 

¹ Laboratoire de Chimie des Matériaux et Catalyse, Faculté des Sciences de Tunis, Université de Tunis El Manar, Campus Farhat Hached, 2092 Tunis, Tunisia; fatma.fakhfakh@fst.utm.tn (F.F.); sahar.raissi@fst.utm.tn (S.R.)

² Department of Chemical Engineering, College of Engineering, Imam Mohammad Ibn Saud Islamic University (IMSIU), Riyadh 11432, Saudi Arabia; kskriaa@imamu.edu.sa (K.K.); bmhadrich@imamu.edu.sa (B.H.)

³ Department of Mechanical and Industrial Engineering, College of Engineering, Imam Mohammad Ibn Saud Islamic University (IMSIU), Riyadh 11432, Saudi Arabia; casmaatki@imamu.edu.sa

⁴ Department of Mechanical Engineering, College of Engineering, University of Ha'il, Ha'il City 81451, Saudi Arabia

* Correspondence: lioua_enim@yahoo.fr

Abstract: The olive mill wastewater (OMW) treatment process is modeled and optimized through new design of experiments (DOE). The first step of the process is coagulation–flocculation using three coagulants (modeled with the mixture design) followed by photo-degradation (modelled with the full factorial design). Based on this methodology, we successfully established a direct correlation between the system's composition during the coagulation–flocculation step and the conditions of the photo-catalytic degradation step. Three coagulants are used in this study, Fe³⁺ solution, lime, and cactus juice, and two parameters are considered for the photo-degradation conditions: dilution and catalyst mass. Utilizing a sophisticated quadratic model, the analysis of the two observed responses reveals the ideal parameters for achieving maximum efficiency in coagulation–flocculation and photo-degradation processes. This is attained using a quasi-equal mixture of limewater and cactus juice, exclusively. To achieve an optimal photo-catalytic degradation, it is essential to maintain a minimal dilution rate while employing an elevated concentration of TiO₂. It was found that the experimental tests validations were in good concordance with the mathematical predictions (a decolorization of 92.57 ± 0.90% and an organic degradation of 96.19 ± 0.97%).

Keywords: olive mill wastewater (OMW); sunlight photo-catalysis; coagulation; lime; cactus; optimization



check for updates

Citation: Fakhfakh, F.; Raissi, S.; Kriaa, K.; Maatki, C.; Kolsi, L.; Hadrich, B. Modeling and Optimization of a Green Process for Olive Mill Wastewater Treatment. *Water* **2024**, *16*, 327. <https://doi.org/10.3390/w16020327>

Academic Editor: Manuel Toledo Padrón

Received: 28 November 2023

Revised: 2 January 2024

Accepted: 14 January 2024

Published: 18 January 2024



Copyright: © 2024 by the authors. Licensee MDPI, Basel, Switzerland. This article is an open access article distributed under the terms and conditions of the Creative Commons Attribution (CC BY) license (<https://creativecommons.org/licenses/by/4.0/>).

1. Introduction

The implementation of any industrial process requires optimization. In this context, the application of the design of experiments (DOE) methodology emerges as an exceptionally robust statistical and mathematical approach, consisting of four main steps: design of the experiments, fitting the model, verifying the model fit quality, and optimization of the studied response. DOE aims to simultaneously study the responses to experimental parameters, overcoming the limitations of traditional experimental approaches that involve parameter exchanges one-by-one, which are often time-consuming and fail to reveal complex variable–response interactions. But even this, DOE, in a simplistic approach, is mostly carried out individually for multi-stage processes. The mixture design, for example, is regularly used for the conception of many real mixtures composed of at least two components to optimize the studied response versus the composition adjustments. Meanwhile, full factorial design creates experimental points using all possible combinations of the levels of the factors in each complete trial or replication of the experiments. Consequently, the synergy between compositional variables and process factors cannot be exhibited. In fact, DOE can be a very useful tool in industrial applications such in the olive oil industry.

The global production of olive oil is experiencing a significant upsurge because of its numerous virtues, as well as its significance as a foodstuff with associated health benefits. According to the international olive oil council, the international production of this product reached 3,398,000 tons in 2022. In the season of 2022/2023, the prices reached a maximum level, with an increase of 40% in the fourth week of March compared with the same period of the previous year. This production is no longer limited to the Mediterranean Basin. Many emergent countries are marking their presence in this field, like Chile (21,000 tons), Australia (19,500 tons), the USA (15,500 tons), and Saudi Arabia (5000 tons). The classical producers like Tunisia (240,000 tons), Turkey (235,000 tons), and Morocco (200,000 tons), classed after the European union, are working on increasing their production. Despite these important contributions to the national economy, it is important to highlight the environmental impact of this industry. It generates approximately 5.4×10^6 m³ of olive mill wastewater (OMW) per year [1]. This quantity can vary depending on different characteristics, such the variety of olive and maturity, climate and soil conditions, and the oil extraction method [2]. For the traditional pressing system involving three-phase centrifugation and continuous de-pitted extraction, the amount of wastewater produced surpasses 47 kg for every 100 kg of olives [3,4]. This agro-industrial effluent presents significant challenges in terms of weight and management complexity [5–7]. It comprises a dark, malodorous, and turbid aqueous liquid containing emulsified grease and a high organic content [8]. More than 80% of its composition includes dissolved sugar, phenols, nitrogen, alcohols, organic acids, pectins, and tannins. Other inorganic materials are also found [9]. The most phytotoxic effect of OMW is related to its high concentration of total phenolic compounds and residual fats responsible for the inhibition of microbial activity [10–13]. Regarding the large quantities produced in short periods of time, the waste generated by this sector significantly contributes to greenhouse gas emissions [14,15]. Particular attention should be considered for its disposal [16], which is regulated by Norm NT106-02.

Certainly, the recovery of valuable compounds such as specific polyphenols, phenols, proteins, fats, cellulose, and lignin from these by-products and their conversion into higher-value products is one of the most efficient alternatives to manage this source of pollution [14,17–19]. But according to Donner et al. [20], the approach of managing this problem via a circular economy is still complex to apply to certain Mediterranean countries like Tunisia and Morocco, as well as France. On the other hand, it is important to relate this question to the context of regions where a scarcity of water constitutes the greatest challenge. In the current Mediterranean context, water recovery constitutes the first priority [21]. Working on saving a greater quantity of water from the oil production process would be the best response to the needs of these highly productive regions. Promising outcomes are being obtained for recovering the best quality and quantity of water through the use of advanced oxidative processes and biological processes [10,11,13,18,22,23]. However, high prices and imposing installation of these processes can sometimes be limiting to their widespread use. Direct evaporation is still the most widely used technique, even though its ecological drawbacks cause the diffusion of bad odors [24–26]. Coagulation-flocculation can be a more effective technology regarding its ease of application and cost-effectiveness. It is frequently used, and it remains a subject for further improvement [27–30]. This technology allows for good removal of suspended solids. The addition of coagulants serves to neutralize the negative charges of oil particles and to decrease the electrostatic repulsion of the electric double layer. Thus, the agglomeration of particles is favorable, and they glide at the interface [31,32]. Commonly, the most widely used coagulants can be metallic, such as aluminum and iron; inorganic, such as lime; or organic, such as polyacrylamide natural compounds including *Moringa oleifera* seeds and cactus [24]. Recently, studies have been more oriented towards the use of a mixture of coagulants to improve the performance of this process [33]. Nevertheless, this technology is still unsatisfactory for obtaining water of acceptable quality. Coagulation–flocculation requires complementary treatments. It generally constitutes the first step of a two- or three-stage treatment process. It can be

followed by biological or oxidative treatments, or even a combination of these two processes [33–35]. Among the advanced oxidative processes, sunlight photo-catalysis shows strong potential for the degradation of organic pollutants due to its low cost and low energy consumption [36].

In this study, a new, green, and low-cost OMW treatment process was designed consisting of two technologies: coagulation–flocculation and sunlight photo-catalysis. In our approach, a combination of coagulant mixture design and a full factorial design was chosen to optimize OMW treatments.

2. Materials and Methods

2.1. Reagents and Materials

Olive mill effluent was received (twenty-four hours after the olive trituration process) from an oil mill.

Cactus rackets were sourced from a local farm at El Manar region (Tunisia). After being rinsed with water and peeled, the pulp was ground into a greenish-yellow liquid and then used without further dilution.

Ferric chloride (99%, Merck) and lime solutions were prepared at a concentration of $1.5 \text{ g} \cdot \text{L}^{-1}$ and $30 \text{ g} \cdot \text{L}^{-1}$, respectively.

The TiO_2 catalyst was synthesized using the sol-gel method, involving the mixing of titanium isopropoxide with isopropanol and acetyl acetate to form the sol. A solution of $0.1 \text{ mol} \cdot \text{L}^{-1}$ nitric acid was used to induce gelation. The resultant gel was calcinated for three hours at 673 K.

2.2. Solid Characterization

The morphology of the solid was investigated using a high-resolution scanning electron microscope from Thermo Fisher Scientific (SEM, 5 kV; 30 kV). The elemental composition was determined using a coupled Energy-Dispersion X-ray (EDX), extending the capabilities of SEM in semi-quantitative detection mode, with a 30 kV acceleration voltage. To conduct X-ray diffraction (XRD), a nickel monochromatic and CuK radiation-based automatic Philips Panalytical diffractometer were used. Comparisons were made between the calculated reticular distances and the Joint Committee on Powder Diffraction Standards (JCPDS) provided with the software used in the Philips Panalytical X-PERT PRO, Dy993 XRPD.

IR spectra were collected using a Perkin Elmer PRAGON 1000 PC FTIR spectrophotometer across a range from 4000 to 400 cm^{-1} . Samples pellets for the FTIR analysis were made by diluting the materials with KBr.

UV-visible spectra in the range of 200 – 900 nm were recorded using a Perkin Elmer spectrophotometer type Instrument lambda 45 linked to an integration sphere type RSA-PE-20 with a speed of $960 \text{ nm} \cdot \text{min}^{-1}$ and an aperture of 4 nm .

2.3. Physico-Chemical Analysis

Prior to use, the OMW was characterized by the following measurements after homogenization. Each measurement was conducted thrice.

The pH was measured according to the description of Rondinini [37]. The dry matter (DM) and ash content (AC), both expressed in $\text{g} \cdot \text{L}^{-1}$, were determined as described by Paredes et al. [38]. The chemical oxygen demand (COD, expressed in $\text{gO}_2 \cdot \text{L}^{-1}$) and the spectrophotometer absorbance (288 nm) were determined following the method adopted by ref. [39].

As described in the previous works of Raissi et al. [40], measuring the decolorization of the solution involves applying an RGB color evaluation. Subsequently, the absorbance is determined using Equation (1):

$$A = \log_{10} \left(\frac{I_0}{I} \right) \quad (1)$$

where the color intensity of the solution is denoted as “ I ”, while the color intensity of water, used as a reference, is represented by “ I_0 ”. This method is also employed for analyzing treated samples and the OMW.

The decolorization (% D) and organic degradation (% OD), representing distinct responses in this study, were accomplished using the following formulas (Equations (2) and (3), respectively):

$$\%D = \frac{\text{Color intensity}_{\text{OMW}}^{\text{initial}} - \text{Color intensity}_{\text{OMW}}^{\text{final}}}{\text{Color intensity}_{\text{OMW}}^{\text{initial}}} \times 100 \quad (2)$$

$$\%OD = \frac{\text{Organic amount}_{\text{OMW}}^{\text{initial}} - \text{Organic amount}_{\text{OMW}}^{\text{final}}}{\text{Organic amount}_{\text{OMW}}^{\text{initial}}} \times 100 \quad (3)$$

2.4. Design of Experiments

The primary objective of the design of experiments (DOE) is to accurately identify the optimal response(s) (dependent variable(s)) depending on multiple factors (as independent variables) simultaneously. This goal could be achieved in a minimum number of experimentally designed runs by using predefined statistical and mathematical design(s) involving model(s) that could predict the experimental response(s). Additionally, we could statistically analyze the quality of the model fit and assess the significance of the influence of each factor and each interaction between them. Mixture design is generally used to identify the optimal response(s) which depend(s) on the composition of the tested mixture, typically consisting of at least two compounds. Nevertheless, the 2^2 full factorial design is commonly employed for analyzing response(s) that could be affected by two factors, each having two levels.

Given our objective to maximize the decolorization (%) and organic degradation (%) of the OMW through a two-step process involving coagulation–flocculation and photocatalysis, we opted to examine all the independent variables that could influence the responses. To achieve this, we employed two specific designs: (1) a simplex-lattice mixture design to ascertain the optimal composition of the flocculant–coagulant used in treating the studied OMW, consisting of lime water (A), Fe^{3+} solution (B), and cactus juice (C)—the materials chosen for this study; and (2) a 2^2 full factorial design to govern the photocatalysis process, influenced by two factors, each with two levels: the mass of TiO_2 (X_1) as a catalyst added to the OMW (with masses of 20 or 40 mg) and the dilution factor (X_2) (at ratios of 1/10 or 2/10). Indeed, using these parameters, the studied process could be classified as green and low-cost.

As shown in Figure 1, the coagulation was carried out by mixing 50 mL of OMW—for which we measured the initial hue and phenol concentration—vigorously with the same volume (50 mL) of a mixture composed of lime water (A), Fe^{3+} solution (B), and cactus juice (C). The mixtures were prepared following the volume ratios specified in columns 2, 3, and 4 of Table 1 using solutions A, B, and C, respectively. The corresponding amount/percentage (and volume) of each mixture composed of those three solutions are presented in Table 1. The photo-catalytic test was carried out on the liquid phase after decantation followed by 1/10 or 2/10 dilution (presenting two levels of factor X_1) and using 20 or 40 mg of TiO_2 (presenting two levels of factor X_2).

After one hour, the mixing operation was halted, and the mixture was transferred into a cylinder for decantation. Over the course of approximately 5 days, decantation was allowed to occur, ensuring a complete separation between the aqueous solution and the sludge. After successful separation, the aqueous solution was diluted with water at a ratio of 1 or 2 mL per 10 mL, describing the first process factor labeled as X_1 . The associated high (1 mL/10 mL) and low (2 mL/10 mL) levels were indicated in Table 1 as coded levels: -1 and $+1$, respectively. Figure 2 shows the positions of all the experiments presented in Table 1.

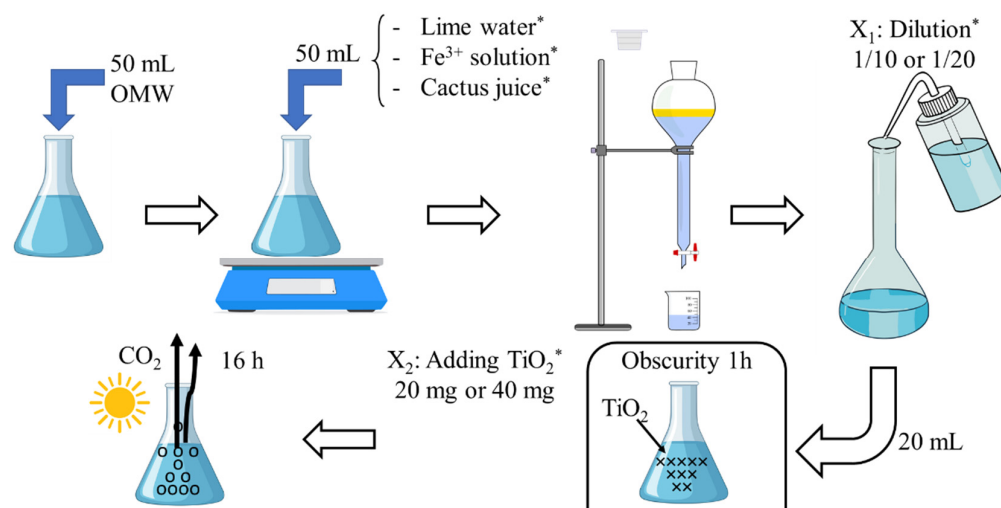


Figure 1. Diagram of the two-step process treatment of OMW. Notes: * Conditions were defined by means of design of experiments (shown in Table 1).

Table 1. Combined design of experiments: mixture design (simplex-lattice; A, B, and C) and full factorial design (2^2 ; X_1 , and X_2).

Run	A * (vol. in mL)	B * (vol. in mL)	C * (vol. in mL)	X_1 ** (Dilution Ratio in mL/mL)	X_2 ** (TiO ₂ Mass in mg)	Decolorization (%)	Organic Degradation (%)
12	0 (0 mL)	1/2 (25 mL)	1/2 (25 mL)	1 (2 mL/10 mL)	-1 (20 mg)	57.14	95.90
4	0 (0 mL)	1 (50 mL)	0 (0 mL)	-1 (1 mL/10 mL)	-1 (20 mg)	97.36	97.60
9	1/2 (25 mL)	1/2 (25 mL)	0 (0 mL)	1 (2 mL/10 mL)	-1 (20 mg)	79.33	96.56
18	0 (0 mL)	1 (50 mL)	0 (0 mL)	-1 (1 mL/10 mL)	1 (40 mg)	66.69	97.92
24	1/2 (25 mL)	0 (0 mL)	1/2 (25 mL)	1 (2 mL/10 mL)	1 (40 mg)	86.65	97.90
7	1/3 (16.7 mL)	1/3 (16.7 mL)	1/3 (16.7 mL)	-1 (1 mL/10 mL)	-1 (20 mg)	90.84	98.02
17	1/2 (25 mL)	0 (0 mL)	1/2 (25 mL)	-1 (1 mL/10 mL)	1 (40 mg)	98.12	98.88
10	1/2 (25 mL)	0 (0 mL)	1/2 (25 mL)	1 (2 mL/10 mL)	-1 (20 mg)	90.53	97.50
6	0 (0 mL)	0 (0 mL)	1 (50 mL)	-1 (1 mL/10 mL)	-1 (20 mg)	79.37	98.18
1	1 (50 mL)	0 (0 mL)	0 (0 mL)	-1 (1 mL/10 mL)	-1 (20 mg)	67.63	99.02
27	0 (0 mL)	0 (0 mL)	1 (50 mL)	1 (2 mL/10 mL)	1 (40 mg)	47.85	96.44
8	1 (50 mL)	0 (0 mL)	0 (0 mL)	1 (2 mL/10 mL)	-1 (20 mg)	92.45	97.94
20	0 (0 mL)	0 (0 mL)	1 (50 mL)	-1 (1 mL/10 mL)	1 (40 mg)	78.75	98.46
13	0 (0 mL)	0 (0 mL)	1 (50 mL)	1 (2 mL/10 mL)	-1 (20 mg)	50.22	96.30
3	1/2 (25 mL)	0 (0 mL)	1/2 (25 mL)	-1 (1 mL/10 mL)	-1 (20 mg)	93.57	98.38
21	1/3 (16.7 mL)	1/3 (16.7 mL)	1/3 (16.7 mL)	-1 (1 mL/10 mL)	1 (40 mg)	76.69	98.46
26	0 (0 mL)	1/2 (25 mL)	1/2 (25 mL)	1 (2 mL/10 mL)	1 (40 mg)	42.94	97.00
14	1/3 (16.7 mL)	1/3 (16.7 mL)	1/3 (16.7 mL)	1 (2 mL/10 mL)	-1 (20 mg)	43.52	96.06
25	0 (0 mL)	1 (50 mL)	0 (0 mL)	1 (2 mL/10 mL)	1 (40 mg)	36.25	95.76
2	1/2 (25 mL)	1/2 (25 mL)	0 (0 mL)	-1 (1 mL/10 mL)	-1 (20 mg)	92.54	98.32
23	1/2 (25 mL)	1/2 (25 mL)	0 (0 mL)	1 (2 mL/10 mL)	1 (40 mg)	75.04	97.28
5	0 (0 mL)	1/2 (25 mL)	1/2 (25 mL)	-1 (1 mL/10 mL)	-1 (20 mg)	83.97	98.10
28	1/3 (16.7 mL)	1/3 (16.7 mL)	1/3 (16.7 mL)	1 (2 mL/10 mL)	1 (40 mg)	41.78	95.98
16	1/2 (25 mL)	1/2 (25 mL)	0 (0 mL)	-1 (1 mL/10 mL)	1 (40 mg)	91.11	98.78
11	0 (0 mL)	1 (50 mL)	0 (0 mL)	1 (2 mL/10 mL)	-1 (20 mg)	40.26	95.80

Table 1. Cont.

Run	A* (vol. in mL)	B* (vol. in mL)	C* (vol. in mL)	X ₁ ** (Dilution Ratio in mL/mL)	X ₂ ** (TiO ₂ Mass in mg)	Decolorization (%)	Organic Degradation (%)
19	0 (0 mL)	1/2 (25 mL)	1/2 (25 mL)	-1 (1 mL/10 mL)	1 (40 mg)	78.57	98.42
22	1 (50 mL)	0 (0 mL)	0 (0 mL)	1 (2 mL/10 mL)	1 (40 mg)	87.32	98.20
15	1 (50 mL)	0 (0 mL)	0 (0 mL)	-1 (1 mL/10 mL)	1 (40 mg)	99.59	99.36

Notes: *: proportion levels (0–1) of mixture design; **: coded variable for X₁ and X₂ of 2² full factorial design; A: lime water (1.5 g · L⁻¹); B: Fe³⁺ solution (30 g · L⁻¹); C: cactus juice (without dilution).

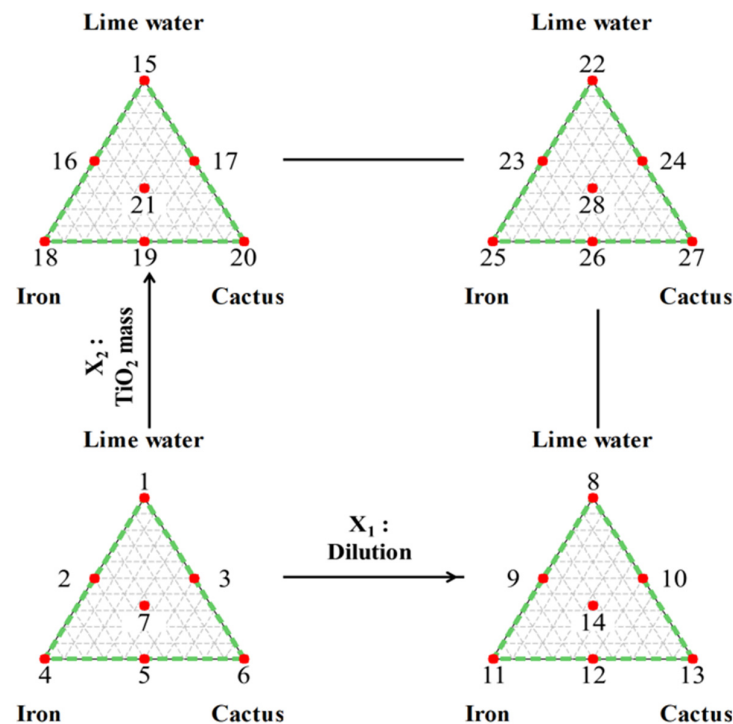


Figure 2. Implemented experimental approach. Combination: simplex-lattice mixture and 2² designs. Notes: Numbers from 1 to 28 represent the runs conditions and positions of design of experiments presented in Table 1.

A volume of 20 mL from the resulting mixture was combined with an appropriate amount of the TiO₂ catalyst for every experimental condition listed in Table 1. Depending on the level selected, the mass changed: 20 mg for the low level (X₂ = -1, Table 1) and 40 mg for the high level (X₂ = +1, Table 1). The solution was then left in dark for one hour, and after that, it was subjected to sunlight exposure for 16 h, during which time the CO₂ emissions were tracked.

The use of Minitab[®] 16.2.1 Software significantly enhanced the efficacy of designing the experiments with 28 trials, as outlined in Table 1, Figures 1 and 2, as well as for deriving the model coefficients. This comprehensive software package was used to proficiently carry out a wide array of statistical tests. It not only computed the optimal responses and corresponding conditions but also seamlessly generated detailed visual representations of the various graphical elements.

We selected decolorization (%) and phenolic compound degradation (%) as responses because of their high significance within this research. This choice underscored the impact of the treatment on the interplay between the effectiveness of decolorization and the reduction in organic substances simultaneously. Equation (4) provides the formulation of the quadratic model that characterized both outcomes. This model functioned in relation to

the constituents of the mixture, namely lime water (A), Fe^{3+} solution (B), and cactus juice (C), as well as the variables of the process, denoted as X_1 (Dilution) and X_2 (TiO_2 mass):

$$\begin{aligned} \hat{y} = & \alpha_1 \cdot x_A + \alpha_2 \cdot x_B + \alpha_3 \cdot x_C + \alpha_{12} \cdot x_A \cdot x_B + \alpha_{13} \cdot x_A \cdot x_C + \alpha_{23} \cdot x_B \cdot x_C \\ & + (\beta_1 \cdot x_A + \beta_2 \cdot x_B + \beta_3 \cdot x_C + \beta_{12} \cdot x_A \cdot x_B + \beta_{13} \cdot x_A \cdot x_C + \beta_{23} \cdot x_B \cdot x_C) \cdot X_1 \quad (4) \\ & + (\chi_1 \cdot x_A + \chi_2 \cdot x_B + \chi_3 \cdot x_C + \chi_{12} \cdot x_A \cdot x_B + \chi_{13} \cdot x_A \cdot x_C + \chi_{23} \cdot x_B \cdot x_C) \cdot X_2 \end{aligned}$$

where:

\hat{y} : the modeled response expressed as a decolorization or organic degradation;

x_A , x_B and x_C : proportions of lime water (A), Fe^{3+} solution (B), and cactus juice (C), respectively; they can take the values of 0, 1/3, 1/2, or 1.

X_1 : the coded value of the dilution factor (independent variable) in the second process;

X_2 : the coded value of the TiO_2 mass as second factor (independent variable) in the second process;

α_i , α_{ij} , β_i , β_{ij} , χ_i , and χ_{ij} : model coefficients.

After the determination of the coefficients for both responses, a statistical study was conducted in order to discuss the fitting quality of the model and determine the responses' maximum simultaneously. The optimization was achieved using the determined model given in Equation (4) with the help of the optimizer tool in the software Minitab® 16.2.1. The corresponding algorithm was implemented to maximize the while using this concept of desirability. The validation of the obtained optimum involving the maximum responses within the same time was conducted experimentally in triplicate using the determined level of each factor.

3. Results and Discussion

3.1. Catalyst Characterization

Figure 3 presents the X-Ray diffraction (XRD) spectrum of TiO_2 , displaying discernible peaks at 2θ (degree) values of 25.3° , 36.9° , 37.9° , 48.1° , 53.9° , 54.9° , and 62.9° . These peaks are in concordance with the patterns found in the [JCPDS card no. 21-1272] for the anatase phase of TiO_2 . Specifically, these peaks correspond to the (101), (103), (004), (112), (200), (105), (211), and (204) crystallographic planes. Additionally, smaller peaks were evident at 2θ angles of 26.9° , 36.1° , 44.9° , 62.7° , and 69.0° , which aligned well with the presence of the rutile phase. The existence of peaks at 25.3° and 48.1° serves as confirmation of the anatase structure of TiO_2 , in agreement with prior studies [41].

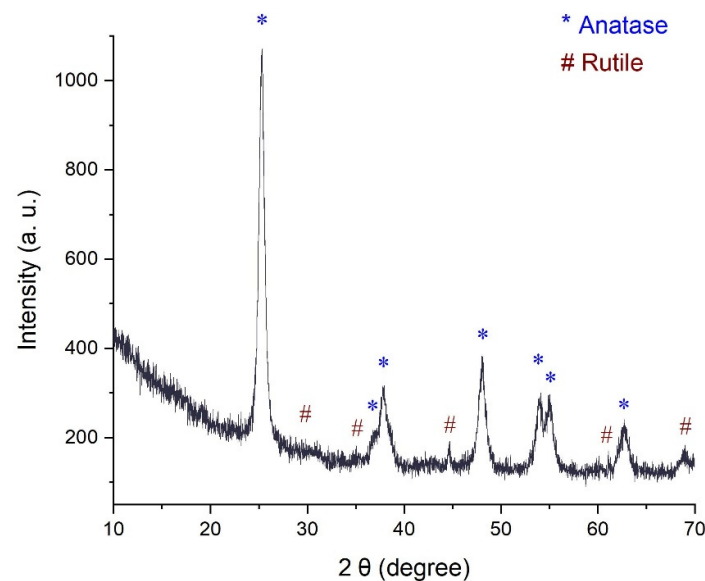


Figure 3. X-Ray diffraction pattern of the catalyst TiO_2 .

SEM was used to describe the morphology of the solid, and EDX spectroscopy was used to identify its elemental composition. Field emission scanning electron microscopy (FE-SEM) was used to examine the morphology of TiO_2 , as shown in Figure 4a, with micro-particles that are noticeably enlarged in size ($\sim 5 \mu\text{m}$). This micrograph shows pebble-like microscopic structures that agglomerate to form larger rocky and non-porous structures. The solid has distinct fissures that are caused by the surface tension that builds up on the pores during evacuation, causing their shrinkage. The EDX results reveal a purity of the solid formed exclusively of titanium and oxygen with residual carbon (Figure 4b).

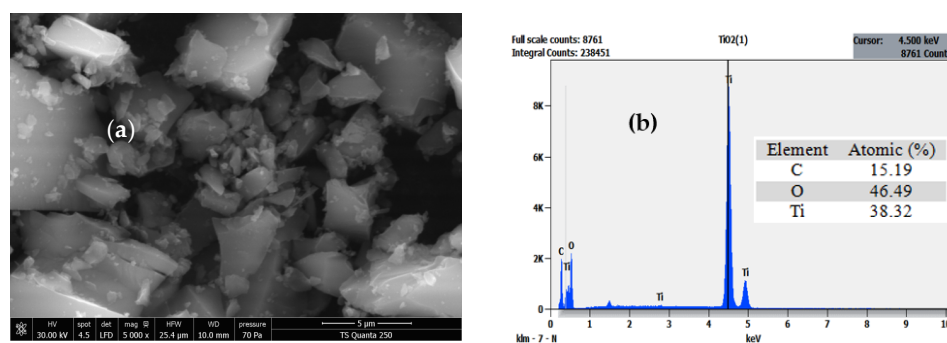


Figure 4. Field emission scanning electron microscopy image (a) and X-Ray diffraction pattern (b) of the catalyst TiO_2 .

In Figure 5, the IR transmission spectra of TiO_2 reveals distinct bands positioned at 435 and 526 cm^{-1} , aligning with the Ti-O stretching and Ti-O-Ti bridging stretching modes inherent in the crystalline lattice of TiO_2 , as previously reported [42,43]. Notably, peaks are also discernible at 795 and 956 cm^{-1} , characteristic of Ti-O-Ti interactions [44]. The presence of bands at 1065 and 1224 cm^{-1} can be ascribed to organic compounds, specifically C-O-C and C-OH functional groups in sol-gel prepared solids, consistent with findings from prior studies [45,46].

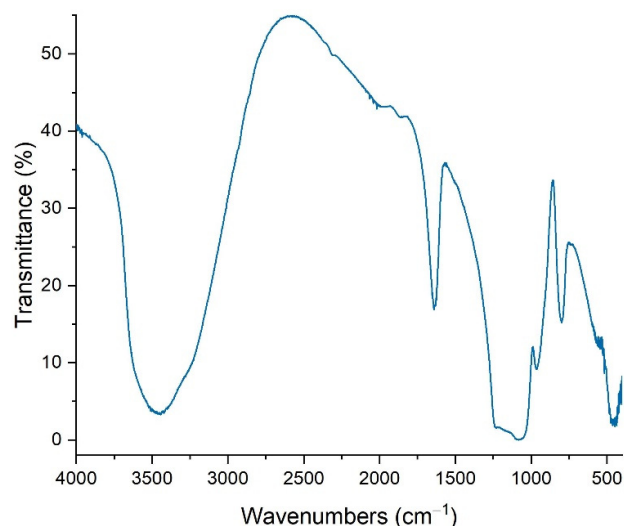


Figure 5. FTIR spectra of TiO_2 .

The broad bands evident at 3401 and 1630 cm^{-1} , frequently observed in the spectra of anatase nanocrystalline TiO_2 , are attributed to the stretching modes of Ti-OH bonds. Additionally, the band spanning between 3292 and 3445 cm^{-1} corresponds to O-H asymmetrical and symmetrical stretching vibrations; a phenomenon that is well-documented in the literature [47,48]. Furthermore, the band situated at 1640 cm^{-1} corresponds to the deformation vibration $\delta_{\text{H-O-H}}$, indicating substantial adsorption of water molecules, in accordance with previous research [47,48].

The optical band gap of the titanium dioxide catalyst was determined utilizing the Kubelka–Munk method, which relies on the calculation of $F(R)$. $F(R)$ is directly proportional to the extinction coefficient (α) and is determined from the Equation (5):

$$F(R) = \frac{(1 - R)^2}{2R} \quad (5)$$

where R represents the reflectance.

Considering an indirect allowed transition for TiO_2 , the band gap energy value could be deduced by plotting $(F(R) \times h\nu)^{1/2}$ against $h\nu$, where h is the Planck constant and ν is the frequency [49].

Figure 6 elucidates the band edge properties of this semiconductor. With a discernible value of approximately 3.2 eV, this measurement is consistent with findings from prior studies [47,48].

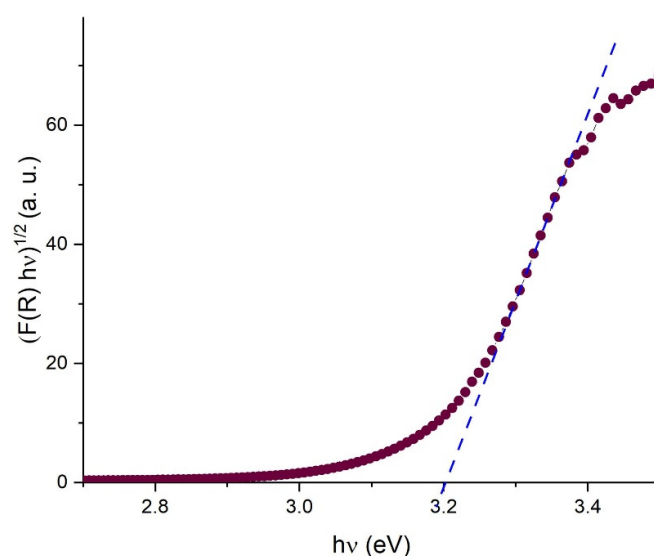


Figure 6. Transformed spectrum reflectance plot for band gap energy determination. The intersection of the blue line with x-axis indicates the band gap energy value.

Our decision to utilize titanium dioxide (TiO_2), synthesized through the sol-gel process, is based on its proven efficacy, as documented in the existing literature (Table 2). This material, when harnessed in the treatment of OMW, consistently exhibited a commendable level of efficiency, particularly when subjected to the stimulating effects of UV light. While its activity under such circumstances is firmly established, the expanding ongoing scientific exploration is now set on a course to amplify its capabilities even further. The focal point of this activity revolves around optimizing this material to harness the abundant energy of sunlight for excitation, a leap that promises to significantly broaden its practicality and effectiveness in various applications.

Table 2. TiO_2 active photo-catalyst.

System	Degradation Yield	Reference
TiO_2 (P25)/UV365 nm	Degradation of 94% phenols; 57% colored compounds	[49]
Carbon-doped TiO_2 /visible light 400–800 nm	More than 80% phenol degradation	[50]
Doped TiO_2 /visible light 400–800 nm	Quantitative degradation of organic compounds	[51]
Nitrogen-doped TiO_2 supported on Zeolite/visible light 400–800 nm	Total degradation of organic compounds	[52]

3.2. OMW Characterization

OMW ranks among the most perilous effluents, presenting substantial environmental risks due to its complex, pollutant-rich composition. Because of the high levels of contaminants such as phenolic chemicals and solid suspension, it is also one of the hardest to treat [5,6]. These compounds are estimated to be present in concentrations of approximately 0.26 to $10.70 \text{ g} \cdot \text{L}^{-1}$, expressed as the gallic acid content [23]. Phenolic compounds are estimated to be present in concentrations of approximately $6.92 \text{ g} \cdot \text{L}^{-1}$ in the treated OMW [53]. The measured pH is approximately 4.62 ± 0.01 . This parameter varies between 4.60 and 6.50 in the literature [49]. The parameters of the studied effluent in this work are COD, ash content, and dry matter. The COD was found to be equal to $52.1 \pm 0.02 \text{ gO}_2 \cdot \text{L}^{-1}$, while the ash content and the dry matter were equal to $17.5 \pm 0.8 \text{ g} \cdot \text{L}^{-1}$ and $108.0 \pm 0.5 \text{ g} \cdot \text{L}^{-1}$, respectively. These values are within the range of those reported in refs. [54–56].

3.3. Coagulation–Flocculation Trials

Given the importance of the effluent’s dry matter concentration, coagulation appears to be the most suitable initial treatment option. This method makes it easier to turn solid suspensions into materials that have been composted or pyrolyzed. Recent studies in this field have revealed a clear trend toward the acceptance of natural ingredients as important participants in the coagulation process, which is consistent with the growing interest in environmentally friendly elements. Among the natural coagulants, notable mentions include chitosane [57], seeds of *Moringa oleifera* [27,58], and cactus [59]. For this study, we opted to use cactus as our flocculent agent; a choice informed by its affordability within the Tunisian context [60] and its straightforward cultivation process.

According to Ndabigengesere and Narasiah [61], the cationic concentration has considerable effects on coagulation, while the anionic impact appears insignificant. In light of this, our exploration delved into the potential enhancement of the cactus’s efficacy when used in combination with lime and ferric solutions. Notably, the utilization of metals for odor reduction, as highlighted by Lagoudianaki et al. [62], reinforced the positive contributions of such elements. The final pH showed differences after the coagulation procedure and decantation, ranging from 5.92 with cactus juice alone to 11.67 when lime alone. A synthesis of Fe^{3+} solution, lime, and cactus juice yielded minimal sludge generation (approximately 48%), while the maximal production of sludge (70%) was observed when relying solely on lime.

The findings after the coagulation–flocculation step, presented in Table 3, demonstrate the variations in the percentage of decolorization and organic compound degradation. The values outlined in Table 3 were derived from the supernatant without any dilution. The coagulation–flocculation using a ternary mixture achieved a phenolic compound degradation of 56.7%, whereas the degradation was higher, reaching 85.4% while employing lime only.

Table 3. Decolorization percentage and organic degradation after the coagulation–flocculation step.

Response	Composition	Lime (50 mL)	Fe^{3+} sol. (50 mL)	Cactus (50 mL)	Lime: Fe^{3+} sol. (25 mL: 25 mL)	Lime:Cactus (25 mL: 25 mL)	Fe^{3+} sol.:Cactus (25 mL: 25 mL)	Lime: Fe^{3+} sol.:Cactus (16.7 mL: 16.7 mL: 16.7 mL)
Decolorization (%)		53.8	14.6	22.8	46.7	60.0	23.9	17.4
Organic degradation (%)		85.4	80.2	83.3	71.0	71.0	84.6	56.7

In terms of decolorization, different trends were observed, with the Fe^{3+} solution yielding the lowest result of 14.6%, while the mixture of cactus and lime achieved the highest decolorization rate of 59.9%. The use of lime alone resulted in a decolorization rate of 53.8%. These results highlight the need for adding lime to the photodegradation process throughout, as well as during the coagulation–flocculation step.

The role of lime in coagulation–flocculation may not be highly effective, but it still contributes significantly to the overall process.

However, this treatment remained insufficient, necessitating further processing for the liquid fraction due to its lingering harmful compounds, particularly soluble polyphenols. Herein, photo-catalysis with sunlight emerges as an economic and effective method that is prominent for its efficiency in effluent treatment. Employing TiO_2 and allowing for a 1 h adsorption period followed by roughly 16 h of daylight in August, the resultant mixtures attained a final pH of approximately 8.50. The COD of the central data point was $7.64 \pm 0.02 \text{ gO}_2 \cdot \text{L}^{-1}$. In terms of gallic acid, the phenolic compounds were remarkably decreased to $0.2 \pm 0.01 \times 10^{-5} \text{ mg} \cdot \text{L}^{-1}$.

This streamlined operational process boasts energy efficiency, capitalizing on the direct and passive utilization of the abundant solar energy accessible within the Mediterranean region. A significant operational challenge encountered in this approach involved ensuring optimal light exposure to the active centers. This goal was achieved through the procedure of flocculation and coagulation, which reduced the suspended matter and solids.

In the quest to model and optimize this dual-stage process, we devised an experimental design that combined a mixture design with a full factorial one. The synergistic application of these two designs enabled an in-depth exploration into the interplay between mixture formulations and independent physic-chemical factors.

3.4. Design of Experiments Results

Table 1 reports the experimental matrix derived from the combination of two kinds of design: a simplex-lattice mixture and 2^2 full factorial designs. All the experiences are regrouped in Figure S1 (Supplementary Materials) before the start and after the achievement of the photo-catalytic process.

This tabulation effectively showcases the intricate interrelationship between the 28 distinct experimental conditions and the two designated responses: decolorization (%) and organic degradation (%).

The decolorization values exhibited a range stretching from 36.25% to 99.59%, with a central tendency characterized by a mean of $73.79 \pm 20.52\%$. Similarly, the spectrum of phenolic compound degradation showed spans between 95.76% and 99.36%, with the average resting at $97.59 \pm 1.09\%$. These outcomes served as a compelling validation of the process's efficacy, particularly in terms of phenolic compound degradation.

Table 4 compiles the results of the *t*-tests for both the decolorization and degradation of phenolic compounds, as well as each coefficient of the model in Equation (4). With regard to decolorization, the results unequivocally underline the sole significant yet negative influence, a consequence of the interaction between the proportion of Fe^{3+} solution (B) and dilution (X_1) ($p < 0.05$). This seemingly counterintuitive effect can be attributed to the original yellow–brown color of the Fe^{3+} (III) solution due to the hexaquaairon (III) ion $[\text{Fe}(\text{H}_2\text{O})_6]^{3+}$ upon undergoing chemical changes [63]. Conversely, in the context of the phenolic compound degradation response, six terms stand out with significant effects ($p < 0.05$): the relative proportions of the constituent components, along with three linear terms representing the interaction between these component proportions and dilution (X_1) ($p < 0.05$). This confluence of findings distinctly underscores the pivotal role played by these factors in driving the degradation of phenolic compounds.

The fitting quality of the model describing the experimental value of decolorization (%), with its coefficients shown in the first column of Table 4, was determined based on four statistical criteria: a high coefficient of correlation ($R^2 = 81.70\%$), an adjusted coefficient of correlation ($R^2_{\text{adj}} = 50.59\%$) very close to 51%, a low RMSE (14.42%—unit of decolorization), and a level of significance ($p = 0.062$, very close to the critical value of significance—0.05). These results allow us to accept the model's fitting of the experimental data of decolorization and to adopt it in this work. The fitting of the model applied to phenolic compound degradation appears to be more powerful than the model applied to decolorization, as evident from the statistical parameters. Specifically, the regression for phenolic compound degradation boasts a substantial level of significance ($p = 0.001 < 0.01$),

a strong coefficient of correlation ($R^2 = 93.71\%$), a high adjusted coefficient of correlation ($R^2_{adj} = 83.03\%$), and a low RMSE (0.448%—unit of phenolic compound degradation) [27].

Table 4. Statistical parameters and model coefficients obtained for the two responses: decolorization and organic degradation.

Term	Decolorization (%)				Organic Degradation (%)			
	Coef.	SE Coef.	<i>t</i>	<i>p</i>	Coef.	SE Coef.	<i>t</i>	<i>p</i>
Component Only								
Linear								
Lime water (A)	88.18	7.18	–	0.054	98.68	0.22	–	<0.001
Fe ³⁺ solution (B)	61.58	7.18	–	0.054	96.82	0.22	–	<0.001
Cactus juice (C)	65.48	7.18	–	0.054	97.39	0.22	–	<0.001
Quadratic								
A × B	15.50	33.02	0.47	0.649	−0.79	1.03	−0.76	0.462
A × C	38.54	33.02	1.17	0.270	−0.22	1.03	−0.21	0.838
B × C	−14.50	33.02	−0.44	0.600	0.27	1.03	0.26	0.801
Component × X ₁ : Dilution								
Linear								
A × X ₁	3.99	7.18	0.56	0.591	−0.53	0.22	−2.38	0.039
B × X ₁	−21.03	7.18	−2.93	0.015	−0.96	0.22	−4.31	0.002
C × X ₁	−14.16	7.18	−1.97	0.077	−0.95	0.22	−4.24	0.002
Quadratic								
A × B × X ₁	−8.83	33.02	−0.27	0.794	−0.73	1.03	−0.71	0.492
A × C × X ₁	−7.81	33.02	−0.24	0.818	0.64	1.03	0.62	0.548
B × C × X ₁	−5.71	33.02	−0.17	0.866	−0.26	1.03	−0.26	0.804
Component × X ₂ : TiO ₂ mass								
Linear								
A × X ₂	6.81	7.184	0.95	0.365	0.17	0.223	0.75	0.469
B × X ₂	−8.57	7.184	−1.19	0.261	0.09	0.223	0.39	0.702
C × X ₂	−0.64	7.184	−0.09	0.930	0.12	0.223	0.55	0.594
Quadratic								
A × B × X ₂	−3.89	33.02	−0.12	0.909	0.38	1.03	0.37	0.718
A × C × X ₂	−13.34	33.02	−0.40	0.695	0.03	1.03	0.03	0.976
B × C × X ₂	−2.86	33.02	−0.09	0.933	0.71	1.03	0.69	0.504

Notes: – Not given by the Minitab® 16.2.1 Software.

Based on the component proportions and process factors, Figure 7 shows the progression of iso-responses for decolorization (Figure 7a) and organic compound degradation (Figure 7b). This graph demonstrates that the decolorization and decomposition of organic compounds are both enhanced by high lime concentrations (>40%).

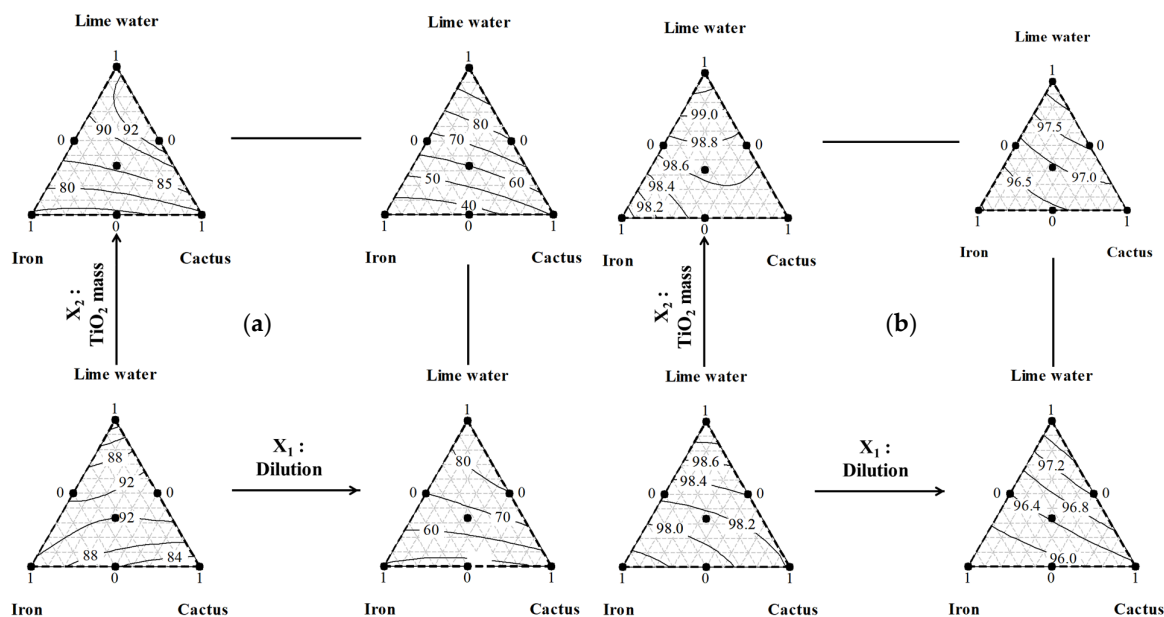
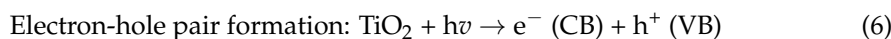


Figure 7. Iso-responses of OMW’s decolorization (a) and organic degradation (b) after treatment utilizing a mixture (composed of lime water, Fe³⁺ solution, and cactus juice) as the coagulant–flocculant and 2 process variables, the dilution rate and TiO₂ mass, as factors influencing the photocatalysis process.

As evident in Figure 7, the positive effect of lime is distinctly observed across all considered dilution levels (X₁) and TiO₂ catalyst masses (X₂). Moreover, the negative effect of the factor dilution rate (X₂) can be clearly observed in Figure 7a for decolorization and in Figure 7b for the organic compound degradation. This is valid for all the factor TiO₂ mass (X₁) levels and all the mixtures. Additionally, the graph demonstrates that the optimal decolorization (>92%) and phenolic compound degradation (>98.5%) percentages are attainable through the application of a low dilution rate (X₁) and either a low or high TiO₂ catalyst mass (X₂). This outcome is achievable by employing a ternary mixture composed predominantly of lime in conjunction with the three utilized components, as emphasized by the research of Karatasios et al. [64].

The contribution of lime to the enhancement of the water treatment process is intricately tied to the significant influence of the solution pH, as expounded by Dong et al., in 2015 [65]. At the heart of this effect lies calcium hydroxide, the primary constituent of lime, which acts as a potent alkaline entity that is able to release two hydroxide ions OH[−]. Consequently, the emergence of the highly reactive OH[•] radical results from augmentation in an alkaline environment. In a classical scenario, the generation of this radical stems from the interaction of water with the positive hole on the valence band, denoted as h⁺ (VB), within TiO₂, as depicted in Equation (6) followed by Equation (7). In an alkaline medium, the direct interaction of the positive hole with OH[−] also contributes to the creation of this active species in alignment with the findings elucidated in Equation (8), as highlighted in the investigations conducted by Karatasios et al. [64].



The Minitab® 16.2.1 Software optimizer was used to find the settings that would maximize both responses simultaneously, as shown in Figures 7–9. This is an important phase, since it finds the ideal levels of each process variable as well as the ideal composition of the ternary mixture. The outcomes of this pure mathematical optimization reaffirm that

the inclusion of iron holds no practical advantage. The apex of coagulation–flocculation efficiency is realized through a blend comprising 48.48% lime and 51.52% cactus juice. Similarly, the paramount outcome in photo-catalytic performance necessitates a low dilution rate and a high mass of TiO₂, as illustrated in Figure 8. Moreover, the desirability to achieve maximum responses was 0.931 and 0.987 for decolorization and organic degradation, respectively (Figure 8). Due to this high desirability, the outcomes for both responses could be considered as highly satisfactory and convergent.

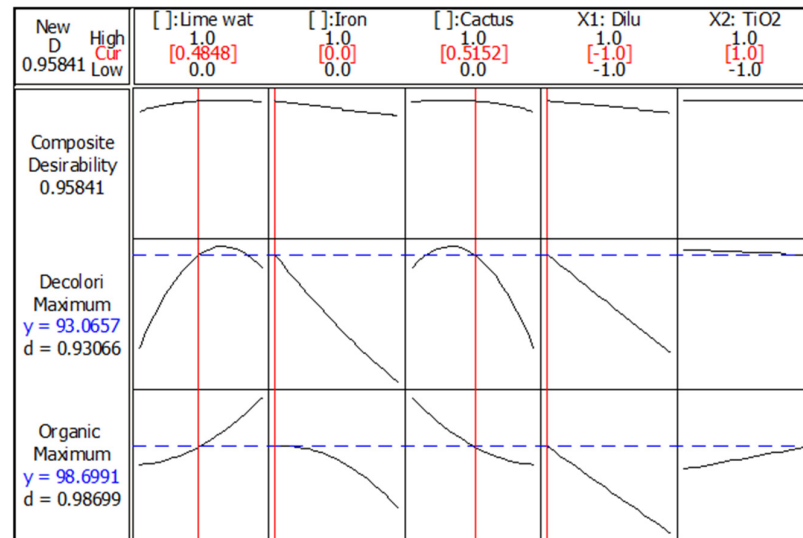


Figure 8. Optimization plot. Dash blue lines indicate the optimum responses simultaneously (written in blue in the right); Continuous red line is useful to determine level of each factor giving the optimum responses (written in red in the top).

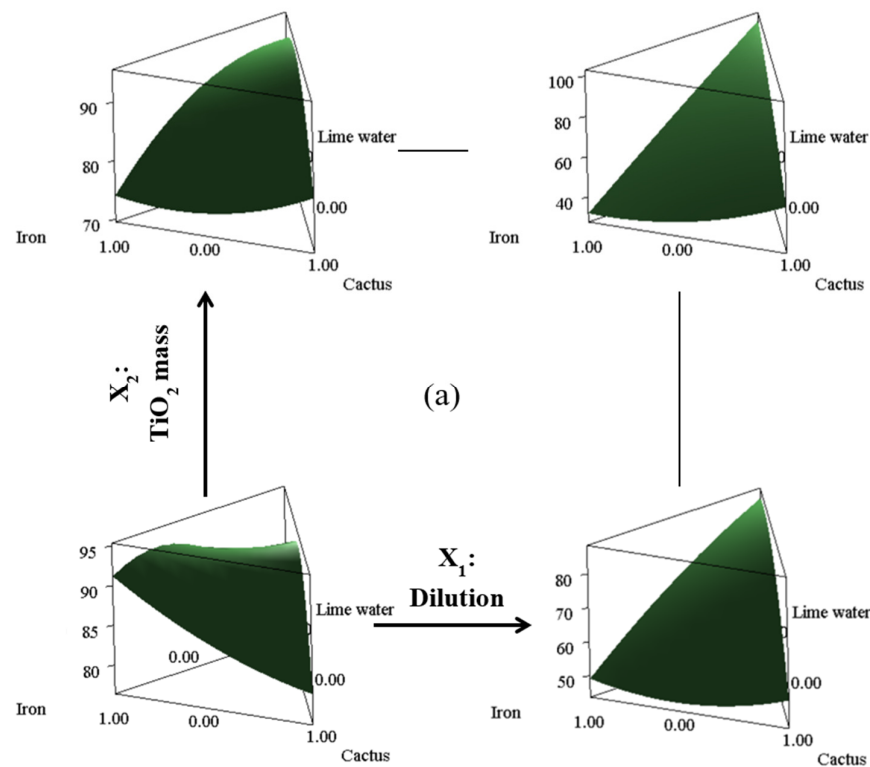


Figure 9. Cont.

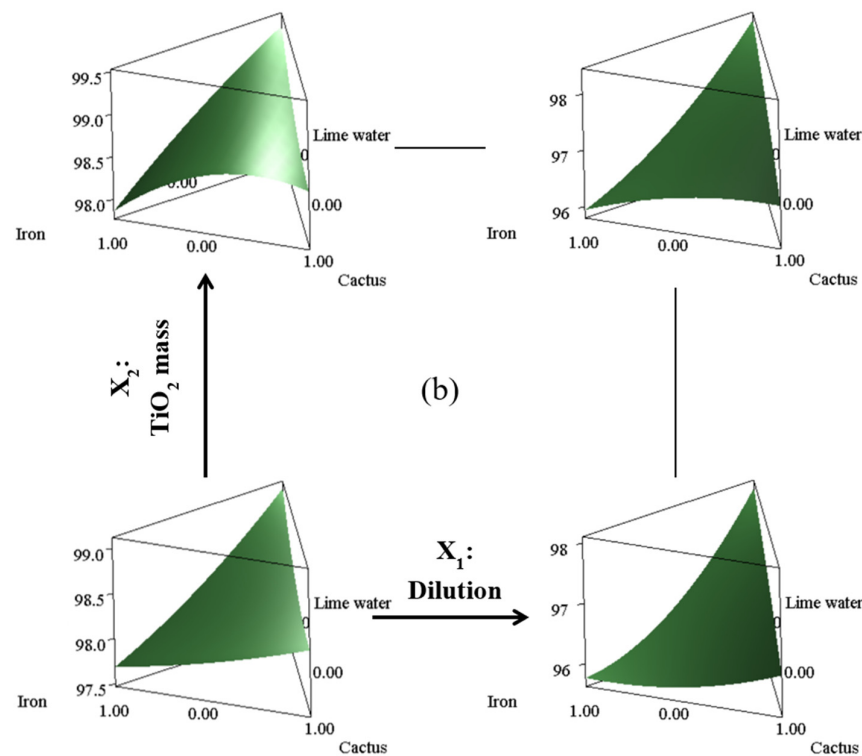


Figure 9. Three-dimensional response surface plot of OMW's decolorization (a) and organic degradation (b) depending on the different variables of the studied two-step process.

4. Conclusions

According to the calculated prediction deduced for this particular combination, as displayed in Figure 9, an optimum result indicating a decolorization of 93.06% and an organic degradation of 98.70% can be achieved. To validate this computed optimum, a series of experimental trials was conducted in triplicate, yielding a decolorization of $92.57 \pm 0.90\%$ and an organic degradation of $96.19 \pm 0.97\%$. These results indicate that the experimental outcomes are replicable given to the low standard deviations and close to the mathematical optimization calculus.

An alternative combination of factors that stands as a strong contender against the determined optimum can be found in the experimental conditions specified in run 15 of Table 1. This scenario involves the utilization of 100% lime, coupled with a low dilution rate and a high TiO_2 mass, culminating in a remarkable decolorization rate of 99.59% and an organic degradation rate of 99.36%. However, despite important achievements in terms of water quality enhancement, this particular solution falls short when considering the magnitude and quality of the generated sludge. Notably, it is worth mentioning that the use of lime as the sole coagulant agent results in the production of the highest quantity of sludge, reaching a substantial value of 69.9%.

Coagulation–flocculation, recognized for its simplicity and cost-effectiveness, brings satisfactory outcomes when dealing with particle-charged wastewater. Its effectiveness when used alone, meanwhile, could occasionally fall short of expectations. Therefore, the goal of our work was to develop a two-stage method combining coagulation–flocculation with sunlight photo-catalysis to increase the effectiveness of this procedure.

A combination of mixture and complete factorial design approaches was used to enhance this original tandem process, focusing on decolorization and phenolic compound degradation by adjusting the composition of the coagulant and the photo-catalytic conditions, respectively. Among the prevalent families of coagulants, metals, lime, and organic agents held our primary focus. Applying the efficiency of the mixture design technique, we methodically investigated the effects caused by iron, lime, and cactus in the area of coagulant composition. We also simultaneously investigated photo-catalytic testing while

modifying the mass of the TiO₂ catalyst and dilution rate at two different levels. Guided by this comprehensive optimization, we pinpointed better conditions: the omission of Fe³⁺ solution and the inclusion of 48.48% lime water and 51.52% cactus juice, coupled with a low dilution rate and a high TiO₂ catalyst mass. Subsequent experimental testing, conducted independently in triplicate, yielded a remarkable decolorization rate of 92.57 ± 0.90% and an organic degradation rate of 96.19 ± 0.97%, close to the mathematical predictions of 93.06% decolorization and 98.70% organic degradation.

A significant decolorization rate of 99.59% and an organic degradation rate of 99.36% were obtained when we investigated the possibility of coagulation using 100% lime. However, this high efficiency came at the cost of generating a considerable amount of sludge, prompting thoughtful consideration from a practical standpoint.

In conclusion, the two-step process involving coagulation–flocculation and sunlight photo-catalysis, optimized by the combination of mixture and full factorial designs methodologies, led to successes in decolorization and organic degradation.

The best conditions we identified, alongside the alternative employment of 100% lime, stress the effectiveness of our treatment approach. However, when assessing the 100% lime approach's overall viability, one must take into account the considerable sludge output generated. The proposed process can be implemented directly within the olive oil plant on site, avoiding the transport step to the wastewater treatment plant. The first step of the process is coagulation–flocculation, which can be conducted using cheap and local Tunisian compounds: cactus juice and lime. The next step is also feasible on-site, since in Tunisia, sunlight is predominant year-round. Therefore, the photocatalysis step is also possible. With this two-stage process, we showed in this study that it is possible to treat olive oil mill wastewater, thus reducing its negative environmental impact while using local and cheap compounds via a green and low-cost process.

Supplementary Materials: The following supporting information can be downloaded at: <https://www.mdpi.com/article/10.3390/w16020327/s1>, Figure S1: Photo of the different experiences of the DOE (a) before sunlight exposure and (b) after 24 h of the photo-catalytic test. C: Cactus; L: Lime; I: Iron; I + L + C: Iron + Lime + Cactus; L + C: Lime + Cactus; I + C: Iron + Cactus; I + L: Iron + Lime; X₁: dilution rate and X₂: TiO₂ Catalyst mass.

Author Contributions: Conceptualization, F.F., S.R., K.K., C.M., L.K. and B.H.; methodology, F.F., S.R., K.K., C.M., L.K. and B.H.; formal analysis, F.F., S.R. and B.H.; investigation, F.F., S.R., K.K., C.M., L.K. and B.H.; writing—original draft, F.F., S.R., K.K., C.M., L.K. and B.H.; writing—review and editing F.F., S.R., K.K., C.M., L.K. and B.H. All authors have read and agreed to the published version of the manuscript.

Funding: This work was supported and funded by the Deanship of Scientific Research at Imam Mohammad Ibn Saud Islamic University (IMSIU) (grant number IMSIU-RG23057).

Data Availability Statement: All the data analyzed during this study are included in this article.

Conflicts of Interest: The authors declare no conflict of interest.

References

1. Hodaifa, G.; Gallardo, P.A.R.; García, C.A.; Kowalska, M.; Seyedsalehi, M. Chemical oxidation methods for treatment of real industrial olive oil mill wastewater. *J. Taiwan Inst. Chem. Eng.* **2019**, *97*, 247–254. [[CrossRef](#)]
2. Sierra, J.; Marti, E.; Montserrat, G.; Cruanas, R.; Garau, M.A. Characterisation and evolution of a soil affected by olive oil mill wastewater disposal. *Sci. Total Environ.* **2001**, *279*, 207–214. [[CrossRef](#)]
3. Cappelletti, G.M.; Ioppolo, G.; Nicoletti, G.M.; Russo, C. Energy requirement of extra virgin olive oil production. *Sustainability* **2014**, *6*, 4966–4974. [[CrossRef](#)]
4. Doula, M.K.; Moreno-Ortego, J.L.; Tinivella, F.; Inglezakis, V.J.; Sarris, A.; Komnitsas, K. Olive Mill Waste: Recent Advances for the Sustainable Development of Olive Oil Industry. In *Olive Mill Waste: Recent Advances for Sustainable Management*; Galanakis, C.M., Ed.; Academic Press: London, UK, 2017; pp. 29–56.
5. Elkadri, A.; Sahnoun, H.; Elfkhi, S.; Abichou, M. Assessing the sustainability of olive mill wastewater storage tank locations in Tunisia. *Euro-Mediterr. J. Environ. Integr.* **2023**, *8*, 255–273. [[CrossRef](#)]

6. Kovačević, M.; Stjepanović, N.; Trigui, S.; Hackenberger, K.D.; Lončarić, Z.; Glavaš, O.G.; Kallel, A.; Hackenberger, B.K. Assessment of adverse effects of olive mill wastewater and olive mill waste contaminated soil on springtail *Folsomia candida*. *Chemosphere* **2022**, *300*, 134651. [CrossRef] [PubMed]
7. Souilem, S.; El-Abbassi, A.; Kiai, H.; Hafidi, A.; Sayadi, S.; Galanakis, C.M. Olive Oil Production Sector: Environmental Effects and Sustainability Challenges. In *Olive Mill Waste: Recent Advances for Sustainable Management*; Galanakis, C.M., Ed.; Academic Press: London, UK, 2017; pp. 1–28.
8. Bombino, G.; Andiloro, S.; Folino, A.; Lucas-Borja, M.E.; Zema, D.A. Short-term effects of olive oil mill wastewater application on soil water repellency. *Agric. Water Manag.* **2021**, *244*, 106563. [CrossRef]
9. Bouaouine, O.; Bourven, I.; Khalil, F.; Baudu, M. Reuse of olive mill wastewater as a bioflocculant for water treatment processes. *J. Clean. Prod.* **2020**, *246*, 119031. [CrossRef]
10. Amor, C.; Lucas, M.S.; García, J.; Dominguez, J.R.; De Heredia, J.B.; Peres, J.A. Combined treatment of olive mill wastewater by Fenton's reagent and anaerobic biological process. *J. Environ. Sci. Health Part A* **2015**, *50*, 161–168. [CrossRef] [PubMed]
11. Khoufi, S.; Louhichi, A.; Sayadi, S. Optimization of anaerobic co-digestion of olive mill wastewater and liquid poultry manure in batch condition and semi-continuous jet-loop reactor. *Bioresour. Technol.* **2015**, *182*, 67–74. [CrossRef] [PubMed]
12. Sanghamitra, P.; Mazumder, D.; Mukherjee, S. Treatment of wastewater containing oil and grease by biological method—A review. *J. Environ. Sci. Health A Toxic Hazard. Subst. Environ. Eng.* **2021**, *56*, 394–412. [CrossRef]
13. Borja, R.; Rincón, B.; Raposo, F.; Alba, J.; Martín, A. A study of anaerobic digestibility of two-phases olive mill solid waste (OMSW) at mesophilic temperature. *Process Biochem.* **2002**, *38*, 733–742. [CrossRef]
14. Velasco-Munoz, J.F.; Mendoza, J.M.F.; Aznar-Sánchez, J.A.; Gallego-Schmid, A. Circular economy implementation in the agricultural sector: Definition, strategies, and indicators. *Resour. Conserv. Recycl.* **2021**, *170*, 105618. [CrossRef]
15. Antonelli, M.; Basile, L.; Gagliardi, F.; Riccaboni, A.; Isernia, P. The AGRIFOODMED Delphi Final Report. Trends, Challenges and Policy Options for Water Management, Farming Systems and Agri-Food Value Chains in 2020–2030; PRIMA Document. 2019. Available online: <http://www.primaitaly.it/wp-content/uploads/2019/06/AGRIFOODMED-Delphi-Final-Report.pdf> (accessed on 13 January 2024).
16. Arvanitoyannis, I.S.; Kassaveti, A. Olive Oil Waste Management: Treatment Methods and Potential Uses of Treated Waste. In *Food Science and Technology, Waste Management for the Food Industries*; Arvanitoyannis, I.S., Ed.; Academic Press: Cambridge, MA, USA, 2008; Chapter 8; pp. 453–568. ISBN 9780123736543. [CrossRef]
17. Donner, M.; Verniquet, A.; Broeze, J.; Kayser, K.; De Vries, H. Critical success and risk factors for circular business models valorizing agricultural waste and by-products. *Resour. Conserv. Recycl.* **2021**, *165*, 105236. [CrossRef]
18. Shabir, S.; Ilyas, N.; Saeed, M.; Bibi, F.; Sayyed, R.Z.; Almalki, W.H. Treatment technologies for olive mill wastewater with impacts on plants. *Environ. Res.* **2023**, *216*, 114399. [CrossRef] [PubMed]
19. Soto, E.R.; Koubaa, M.; Moubarik, A.; Lopes, R.P.; Saraiva, J.A.; Boussetta, N.; Grimi, N.; Barba, F.J. Emerging opportunities for the effective valorisation of wastes and by-products generated during olive oil production process: Non-conventional methods for the recovery of high-added value compounds. *Trends Food Sci. Technol.* **2015**, *45*, 296–310. [CrossRef]
20. Donner, M.; Erraach, Y.; López-i-Gelats, F.; Manuel-I Martin, J.; Yatribi, T.; Radić, I.; El Hadad-Gauthier, F. Circular bioeconomy for olive oil waste and by-product valorisation: Actors' strategies and conditions in the Mediterranean area. *J. Environ. Manag.* **2022**, *321*, 115836. [CrossRef] [PubMed]
21. Fersi, C.; Ben Salah, I.; Medimagh, R. Circular Economy in Tunisia. In *Circular Economy: Recent Trends in Global Perspective*; Ghosh, S.K., Ghosh, S.K., Eds.; Springer Nature: Singapore, 2021; Chapter 4. [CrossRef]
22. Jarbouli, R.; Hadrich, B.; Gharsallah, N.; Ammar, E. Olive mill wastewater disposal in evaporation ponds in Sfax (Tunisia): Moisture content effect on microbiological and physical chemical parameters. *Biodegradation* **2009**, *20*, 845–858. [CrossRef]
23. Khoufi, S.; Aloui, F.; Sayadi, S. Pilot scale hybrid process for olive mill wastewater treatment and reuse. *Chem. Eng. Process.* **2009**, *48*, 643–650. [CrossRef]
24. Achak, M.; Boumya, W.; Elamraoui, S.; Asdiou, N.; Taoufik, N.; Barka, N.; Aboulkas, A.; Lamy, E. Performance of olive mill wastewater treatment using hybrid system combining sand filtration and vertical flow constructed wetlands. *J. Water Process Eng.* **2023**, *53*, 103737. [CrossRef]
25. Martínez-Gallardo, M.R.; López, M.J.; Jurado, M.M.; Suárez-Estrella, F.; López-González, J.A.; Sáez, J.A.; Moral, R.; Moreno, J. Bioremediation of Olive Mill Wastewater sediments in evaporation ponds through in situ composting assisted by bioaugmentation. *Sci. Total Environ.* **2020**, *703*, 135537. [CrossRef] [PubMed]
26. El Hassani, F.Z.; El Karkouri, A.; Errachidi, F.; Merzouki, M.; Benlemlih, M. The impact of Olive Mill Wastewater spreading on soil and plant in arid and semi-arid areas. *Environ. Nanotechnol. Monit. Manag.* **2023**, *20*, 100798. [CrossRef]
27. Rifaia, S.K.; Souabia, S.; El Felsb, L.; Driouicha, A.; Nassrid, I.; Haddajia, C.; Hafidi, M. Optimization of coagulation process for treatment of olive oil mill wastewater using *Moringa oleifera* as a natural coagulant, CCD combined with RSM for treatment optimization. *Process Saf. Environ. Prot.* **2022**, *162*, 406–418. [CrossRef]
28. Gandiwa, B.I.; Moyo, L.B.; Ncube, S.; Mamvura, T.A.; Mguni, L.L.; Hlabangana, N. Optimisation of using a blend of plant based natural and synthetic coagulants for water treatment: (*Moringa Oleifera*-*Cactus Opuntia*-alum blend). *S. Afr. J. Chem. Eng.* **2020**, *34*, 158–164. [CrossRef]
29. El Shahawy, A.; Hassan, S.; Ebrahiem, E.E.; El Kersh, I. Organic pollutants removal from olive mill wastewater by coagulation and electrocoagulation: Application of Box-Behnken design (BBD). *Desalin. Water Treat.* **2019**, *148*, 102–118. [CrossRef]

30. Vuppala, S.; Shaik, R.U.; Stoller, M. Multi-response optimization of coagulation and flocculation of olive mill wastewater: Statistical approach. *Appl. Sci.* **2021**, *11*, 2344. [[CrossRef](#)]
31. Villaseñor-Basulto, D.L.; Astudillo-Sánchez, P.D.; del Real-Olvera, J.; Bandala, E.R. Wastewater treatment using *Moringa oleifera* Lam seeds: A review. *J. Water Process Eng.* **2018**, *23*, 151–164. [[CrossRef](#)]
32. Zhang, Z. The flocculation mechanism and treatment of oily wastewater by flocculation. *Water Sci. Technol.* **2017**, *76*, 2630–2637. [[CrossRef](#)]
33. Sher, F.; Malik, A.; Liu, H. Industrial polymer effluent treatment by chemical coagulation and flocculation. *J. Environ. Chem. Eng.* **2013**, *1*, 684–689. [[CrossRef](#)]
34. Aouan, B.; Alehyen, S.; Fadil, M.; El Alouani, M.; Saufi, H.; El Herradi, E.H.; El Makhoukhi, F.; Taibi, M. Development and optimization of geopolymer adsorbent for water treatment: Application of mixture design approach. *J. Environ. Manag.* **2023**, *338*, 117853. [[CrossRef](#)]
35. Aragaw, T.A.; Bogale, F.M. Role of coagulation/flocculation as a pretreatment option to reduce colloidal/bio-colloidal fouling in tertiary filtration of textile wastewater: A review and future outlooks. *Front. Environ. Sci.* **2023**, *11*, 1142227. [[CrossRef](#)]
36. Fan, X.; Liu, X.; Wang, Y. Low-cost and resource-efficient monolithic photocatalyst with enhanced solar light utilization for the photocatalytic treatment of organic wastewater. *Chemosphere* **2023**, *312*, 137052. [[CrossRef](#)] [[PubMed](#)]
37. Rondinini, S. pH measurements in non-aqueous and aqueous-organic solvents-definition standard procedures. *Anal. Bioanal. Chem.* **2002**, *374*, 813–816. [[CrossRef](#)]
38. Paredes, C.; Cegarra, J.; Roig, A.; Sánchez-Monedero, M.A.; Bernal, M.P. Characterization of olive mill wastewater (alpechin) and its sludge for agricultural purposes. *Bioresour. Technol.* **1999**, *67*, 111–115. [[CrossRef](#)]
39. Nassar, N.N.; Arar, L.A.; Marei, N.N.; Abu Ghanim, M.M.; Dwekat, M.S.; Sawalha, S.H. Treatment of olive mill based wastewater by means of magnetic nanoparticles: Decolourization, dephenolization and COD removal. *Environ. Nanotechnol. Monit. Manag.* **2014**, *1–2*, 14–23. [[CrossRef](#)]
40. Raissi, S.; Fakhfakh, F. Analytical validation of smartphone spectroscopic technic used in an educational kinetic study. *Int. J. Anal. Chem.* **2023**, *2023*, 3729633. [[CrossRef](#)]
41. Ba-Abbad, M.; Kadhum, A.; Mohamad, A.; Takriff, M.S.; Sopian, K. Synthesis and catalytic activity of TiO₂ nanoparticles for photochemical oxidation of concentrated chlorophenols under direct solar radiation. *Int. J. Electrochem. Sci.* **2012**, *7*, 4871–4888. [[CrossRef](#)]
42. Wang, G.; Xu, L.; Zhang, J.; Yin, T.; Han, D. Enhanced photocatalytic activity of TiO₂ powders (P25) via calcination treatment. *Int. J. Photoenergy* **2012**, *2012*, 265760. [[CrossRef](#)]
43. Kanakaraju, D.; Wong, S.P. Photocatalytic efficiency of TiO₂-biomass loaded mixture for wastewater treatment. *J. Chem.* **2018**, *2018*, 4314969. [[CrossRef](#)]
44. Qourzal, S.; Barka, N.; Tamimi, M.; Assabbane, A.; Nounah, A.; Ihlal, A.; Ait-ichou, Y. Sol-gel synthesis of TiO₂-SiO₂ photocatalyst for β-naphthol photodegradation. *Mater. Sci. Eng. C* **2009**, *29*, 1616–1620. [[CrossRef](#)]
45. León, A.; Reuquen, P.; Garín, C.; Segura, R.; Vargas, P.; Zapata, P.; Orihuela, P.A. FTIR and raman characterization of TiO₂ nanoparticles coated with polyethylene glycol as carrier for 2-methoxyestradiol. *Appl. Sci.* **2017**, *7*, 49. [[CrossRef](#)]
46. Zhang, X.; Wang, N.; Li, J.; Xia, Q.; Meng, J.; Dingb, J.; Lu, J. Synthesis and characterization of TiO₂/graphene oxide nanocomposites for photoreduction of heavy metal ions in reverse osmosis concentrate. *RSC Adv.* **2018**, *8*, 34241–34251. [[CrossRef](#)] [[PubMed](#)]
47. Bezrodna, Y.; Puchkovska, G.; Shymanovska, V.; Baran, J.; Ratajczak, H. IR-analysis of H-bonded H₂O on the pure TiO₂ surface. *J. Mol. Struct.* **2004**, *700*, 175. [[CrossRef](#)]
48. Chen, J.; Zhang, L. NH₄Cl-assisted low temperature synthesis of anatase TiO₂ nanostructures from Ti powder. *J. Mater. Lett.* **2009**, *63*, 1797–1799. [[CrossRef](#)]
49. López, R.; Gómez, R. Band-gap energy estimation from diffuse reflectance measurements on sol-gel and commercial TiO₂: A comparative study. *J. Sol-Gel Sci. Technol.* **2012**, *61*, 1–7. [[CrossRef](#)]
50. El Hajjouji, H.; Barje, F.; Pinelli, E.; Bailly, J.R.; Richard, C.; Winterton, P.; Revel, J.C.; Hafidi, M. Photochemical UV/TiO₂ treatment of olive mill wastewater (OMW). *Bioresour. Technol.* **2008**, *99*, 7264–7269. [[CrossRef](#)]
51. Li, Y.; Qin, Z.; Guo, H.; Yang, H.; Zhang, G.; Ji, S.; Zeng, T. Low-temperature synthesis of anatase TiO₂ nanoparticles with tunable surface charges for enhancing photocatalytic activity. *PLoS ONE* **2014**, *9*, e114638. [[CrossRef](#)] [[PubMed](#)]
52. Barba-Nieto, I.; Caudillo-Flores, U.; Fernández-García, M.; Kubacka, A. Sunlight-operated TiO₂-based photocatalysts. *Molecules* **2022**, *25*, 4008. [[CrossRef](#)]
53. Speltini, F.; Maraschi, A.; Sturini, M.; Caratto, V.; Ferretti, M.; Profumo, A. Sorbents coupled to solar light TiO₂-based photocatalysts for olive mill wastewater treatment. *Int. J. Photoenergy* **2016**, *2016*, 8793841. [[CrossRef](#)]
54. Hanafi, F.; Belaoufi, A.; Mountadar, M.; Assobhei, O. Augmentation of biodegradability of olive mill wastewater by electrochemical pre-treatment: Effect on phytotoxicity and operating cost. *J. Hazard. Mater.* **2011**, *190*, 94–99. [[CrossRef](#)]
55. Al-Essa, K. Activation of Jordanian bentonite by hydrochloric acid and its potential for olive mill wastewater enhanced treatment. *J. Chem.* **2018**, *2018*, 8385692. [[CrossRef](#)]
56. Elayadi, F.; Achak, M.; Beniich, N.; El Adlouni, C. Factorial design for optimizing and modeling the removal of organic pollutants from olive mill wastewater using a novel low-cost bioadsorbent. *Water Air Soil Pollut.* **2020**, *231*, 351. [[CrossRef](#)]

57. Patel, H.; Vashi, R.T. Comparison of naturally prepared coagulants for removal of COD and color from textile wastewater. *Glob. Nest J.* **2013**, *15*, 522–528.
58. Rasheed, F.A.; Alkaradaghi, K.; Al-Ansari, N. The potential of *Moringa oleifera* seed in water coagulation-flocculation technique to reduce water turbidity. *Water Air Soil Pollut.* **2023**, *234*, 250. [[CrossRef](#)]
59. Oladoja, N.A. Advances in the quest for substitute for synthetic organic polyelectrolytes as coagulant aid in water and wastewater treatment operations. *Sustain. Chem. Pharm.* **2016**, *3*, 47–58. [[CrossRef](#)]
60. Louhaichi, M.; Hamdeni, I.; Slim, S.; Hassen, S.; Harberg, S.; Gouhis, F. Economic valuation of cactus pear production in semi-arid regions of Tunisia. *Acta Hort.* **2022**, *1343*, 97–102. [[CrossRef](#)]
61. Ndabigengesere, K.; Narasiah, S. Influence of operating parameters on turbidity removal by coagulation with *Moringa oleifera* seeds. *Environ. Technol.* **1996**, *17*, 1103–1112. [[CrossRef](#)]
62. Yazdanbakhsh, A.; Mehdipour, F.; Eslami, A.; Maleksari, H.S.; Ghanbari, F. The combination of coagulation, acid cracking and Fenton-like processes for olive oil mill wastewater treatment: Phytotoxicity reduction and biodegradability augmentation. *Water Sci. Technol.* **2015**, *71*, 1097–1105. [[CrossRef](#)] [[PubMed](#)]
63. Miliordos, E.; Xantheas, S.S. Ground and Excited States of the $[\text{Fe}(\text{H}_2\text{O})_6]^{2+}$ and $[\text{Fe}(\text{H}_2\text{O})_6]^{3+}$ Clusters: Insight into the Electronic Structure of the $[\text{Fe}(\text{H}_2\text{O})_6]^{2+}$ – $[\text{Fe}(\text{H}_2\text{O})_6]^{3+}$ Complex. *J. Chem. Theory Comput.* **2015**, *11*, 1549–1563. [[CrossRef](#)]
64. Karatasios, I.; Katsiotis, M.S.; Likodimos, V.; Kontos, A.I.; Papavassiliou, G.; Falaras, P.; Kilikoglou, V. Photo-induced carbonation of lime-TiO₂ mortars. *Appl. Catal. B Environ.* **2010**, *95*, 78–86. [[CrossRef](#)]
65. Dong, H.; Zeng, G.; Tang, L.; Fan, C.; Zhang, C.; He, X.; He, Y. An overview on limitations of TiO₂-based particles for photocatalytic degradation of organic pollutants and the corresponding countermeasures. *Water Res.* **2015**, *79*, 128–146. [[CrossRef](#)] [[PubMed](#)]

Disclaimer/Publisher’s Note: The statements, opinions and data contained in all publications are solely those of the individual author(s) and contributor(s) and not of MDPI and/or the editor(s). MDPI and/or the editor(s) disclaim responsibility for any injury to people or property resulting from any ideas, methods, instructions or products referred to in the content.